# LETTERS

# Global estimate of aerosol direct radiative forcing from satellite measurements

Nicolas Bellouin[1], Olivier Boucher[1], Jim Haywood[1] & M. Shekar Reddy[2]

**Atmospheric aerosols cause scattering and absorption of incoming solar radiation. Additional anthropogenic aerosols released into the atmosphere thus exert a direct radiative forcing on the climate system[1]. The degree of present-day aerosol forcing is estimated from global models that incorporate a representation of the aerosol cycles[1–3]. Although the models are compared and validated against observations, these estimates remain uncertain. Previous satellite measurements of the direct effect of aerosols contained limited information about aerosol type, and were confined to oceans only[4,5]. Here we use state-of-the-art satellite-based measurements of aerosols[6–8] and surface wind speed[9] to estimate the clear-sky direct radiative forcing for 2002, incorporating measurements over land and ocean. We use a Monte Carlo approach to account for uncertainties in aerosol measurements and in the algorithm used. Probability density functions obtained for the direct radiative forcing at the top of the atmosphere give a clear-sky, global, annual average of $-1.9\,\mathrm{W\,m^{-2}}$ with standard deviation, $\pm0.3\,\mathrm{W\,m^{-2}}$. These results suggest that present-day direct radiative forcing is stronger than present model estimates, implying future atmospheric warming greater than is presently predicted, as aerosol emissions continue to decline[10].**

Anthropogenic biomass burning and industrial pollution aerosols are primarily emitted from agriculture and industry, although some biomass-burning emissions are due to naturally occurring large-scale fires in tropical and boreal regions. Natural aerosols are mostly mineral dust and marine aerosols, although some of the mineral dust emissions are due to human changes in land use. The aerosol direct radiative forcing (DRF) is defined as the perturbation of the radiative fluxes caused by anthropogenic aerosols (natural aerosols are not included). To obtain an estimate of the DRF, a measure of the anthropogenic aerosol loading and knowledge of their size distributions and refractive indices are needed. Remote-sensing measurements determine the total aerosol loading via the aerosol optical thickness (AOT), which is a measure of the wavelength-dependent aerosol extinction in the atmospheric column. Size distributions and refractive indices are determined from *in situ* measurements and used to compute the aerosol optical properties. The Moderate Resolution Imaging Spectrometer (MODIS) space instrument has operated onboard the Terra and Aqua platforms since December 1999 and May 2002, respectively. It provides the total AOT at 0.55 μm for clear-sky conditions over oceans and land surfaces[6,7], excluding deserts and snow-covered areas where the contribution from the surface to the measured signal is too large for accurate retrievals.

Determining the anthropogenic AOT from the total AOT requires additional information. The accumulation-mode fraction (AMF) is the fraction of the AOT from aerosols smaller than 1 μm in diameter (called accumulation-mode aerosols). The AMF is successfully retrieved by MODIS over oceans. Figure 1 presents airborne and
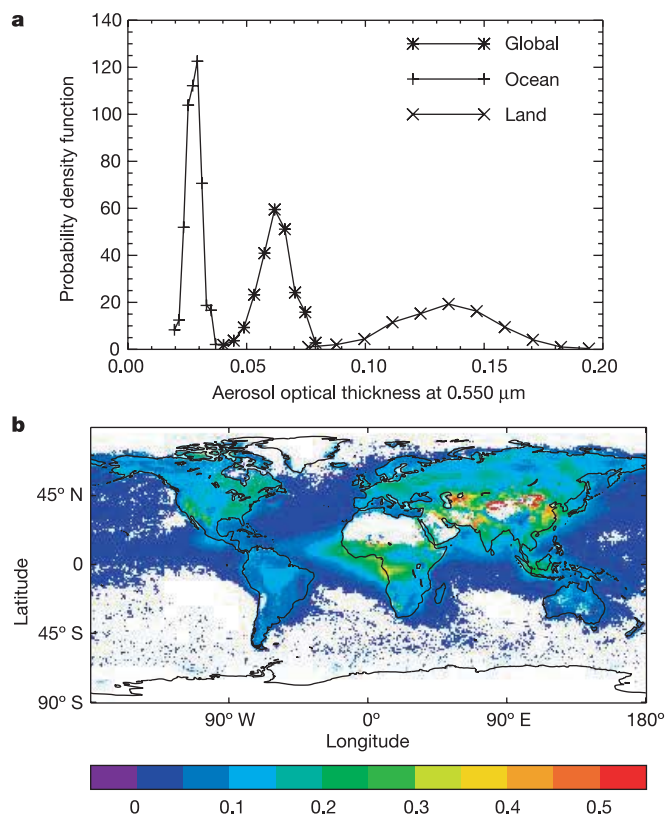
ground-based measurements of the AMF. Airborne measurements were made using Particle System Measurement probes by the Met Office C130 and FAAM BAe146 aircraft during the TARFOX and ADRIEX (industrial aerosols from North America and Italy, respectively), ACE-2 (pollution reaching the North Atlantic), SHADE (mineral dust from Sahara reaching Senegal and Capo-Verde), JET-2000 (mixture of mineral dust and biomass-burning in the gulf of Guinea), and SAFARI-2000 (biomass-burning in Namibia) field campaigns[11].

Sun-photometer measurements are from an analysis of several high-quality sites of the Aerosol Robotic Network (AERONET)[12]. Natural aerosols alone are associated with AMFs smaller than $0.35 \pm 0.05$. (From here on, the uncertain parameters are assumed to follow a gaussian distribution. Estimates of the mean value and the standard deviation are given.) Anthropogenic aerosols alone are associated with AMFs larger than $0.83 \pm 0.05$. AMFs within these two boundaries are associated with mixtures of anthropogenic and natural aerosols. In such cases, the presence of a mixture of mineral dust and biomass-burning aerosols is implied by a significant TOMS (Total Ozone Mapping Spectrometer) aerosol index[8], which includes only those aerosols that absorb in the ultraviolet, that is, mineral dust and biomass-burning aerosols. The AMF retrieved by MODIS is
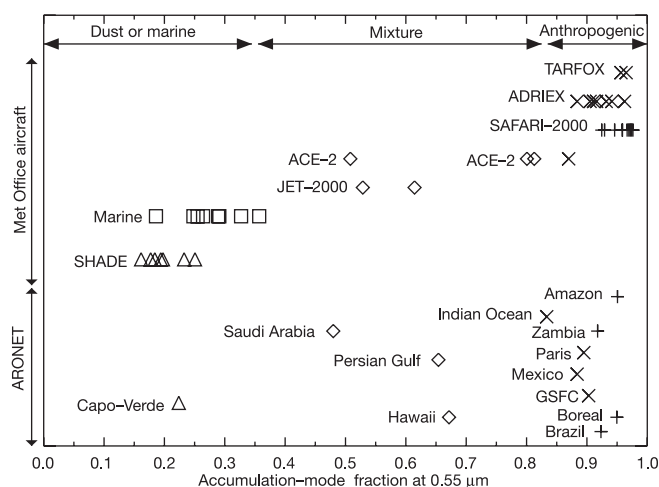


**Figure 1** | *In situ* **observations of the AMF.** AMF at 0.55 μm as measured by the Met Office and FAAM aircraft during several field campaigns (top) and by the AERONET sun-photometers at selected sites[12]. Measurements dominated by pollution aerosols are indicated by crosses, biomass-burning aerosols by plus signs, mixtures of marine and/or mineral dust and/or anthropogenic aerosols by diamonds, marine aerosols by squares and mineral dust by triangles. Airborne measurements of marine aerosols come from flights operated in clean atmospheric conditions.

[1]Met Office, Exeter EX1 3PB, UK. [2]NOAA Geophysical Fluid Dynamics Laboratory, Princeton, New Jersey 08540, USA.

**Figure 2 | Anthropogenic AOT at 0.55 μm. a**, PDFs of the annual, global average over ocean, land and globally. **b**, Distribution for the year 2002. This is the mean of 250 experiments.

translate into a narrow PDF, centred at an average AOT of 0.03 with a standard deviation of 0.003. The smaller accuracy of the MODIS AOT and the necessary use of models widen the PDF and the AOT over land is 0.13 ± 0.02. On a global average, we estimate anthropogenic aerosols to have an AOT of 0.06 ± 0.01. The annual distribution of the anthropogenic AOT, defined as the mean of our ensemble experiments and shown in Fig. 2b, illustrates the identification of the anthropogenic industrial pollution and biomass-burning aerosols achieved by the algorithm. Anthropogenic aerosols are shown to be significant contributors to the total AOT over oceans downwind of major biomass-burning events in central and southern Africa, and off the coasts of North America, Europe, China and India. Over land, largest AOTs are observed in the biomass-burning areas of Africa and South America, and the large industrial emissions from China and India are also apparent. We also note that the continuity between land and ocean is good, although not perfect.

The aerosol size distributions and refractive indices needed to convert the anthropogenic AOT to the DRF at the top of the atmosphere and at the surface are taken from AERONET measurements[12]. A representative AERONET site is assigned to each of the above six regions (Table 1). The single-scattering albedo (SSA), defined as the ratio of scattering to extinction, is also shown. The most absorbing aerosols, corresponding to the smallest SSAs, are found in the biomass-burning regions and developing countries. The use of a single site to characterize a large region may seem unjustified: however, according to our analysis of AERONET sites, SSAs in the African and South American regions range from 0.85 to 0.91 and 0.89 to 0.94, respectively. The standard deviations used in the Monte Carlo approach encompass this regional variability as well as measurement errors. The PDFs for the DRF are presented in Fig. 3. The clear-sky DRF is $-1.9 \pm 0.3\,\mathrm{W\,m^{-2}}$ at the top of the atmosphere, and $-4.4 \pm 0.6\,\mathrm{W\,m^{-2}}$ at the bottom of the atmosphere, on a global average. The uncertainty in the DRF is due to the uncertainty in the anthropogenic AOT, but also to the uncertainty in the aerosol SSA. The largest DRFs are over land surfaces, implying that much work is needed to improve satellite retrievals over such surfaces. The difference between the top of the atmosphere and surface DRF corresponds to the energy absorbed in the aerosol layer, which amounts to $2.5\,\mathrm{W\,m^{-2}}$ for our best, clear-sky estimate.

We can approximate the all-sky DRF by assuming that the cloudy-sky contribution is negligible. Hence, the all-sky DRF is simply the clear-sky DRF multiplied by the clear-sky fraction (or one minus the cloud fraction). Using the MODIS cloud fraction[17], the all-sky DRF is $-0.8 \pm 0.1\,\mathrm{W\,m^{-2}}$ at the top of the atmosphere, and $-1.9 \pm 0.2\,\mathrm{W\,m^{-2}}$ at the surface. In fact, the cloudy-sky contribution is likely to be either negligible for scattering aerosols or positive for absorbing aerosols above cloud[18]. The all-sky DRF is then certainly less negative than our estimate of $-0.8\,\mathrm{W\,m^{-2}}$, but this value cannot be improved until satellite observations supply the vertical profiles of aerosol and clouds.

The clear-sky DRF does not suffer from assumptions in the

unfortunately not considered reliable over land surfaces. Five global models, including aerosol representations[2,13–16] and using the same aerosol emissions, show that 47 ± 9% of the AOT over land is due to anthropogenic aerosols, on a global, annual average. To account for regional differences, we use different anthropogenic fractions over the six regions of our analysis (see Methods and Table 1). The standard deviation of the anthropogenic fraction is large for most of the regions, reflecting uncertainties in modelling aerosol transport and removal.

Uncertainties also exist in satellite products and algorithm parameters. For this reason, we do not give a single estimate of the anthropogenic AOT and DRF, but estimate probability density functions (PDFs) obtained from a Monte Carlo approach. Such a PDF is presented on Fig. 2a for the anthropogenic AOT from a set of 250 experiments. Over oceans, the relative accuracy of the MODIS aerosol algorithm and the robustness of the identification algorithm

**Table 1 | Regional boxes used in the anthropogenic DRF estimation**

| | Boundaries | Anthropogenic fraction over land | AERONET site | SSA at 0.55 μm |
|---|---|---|---|---|
| North America | 90° N–30° N 180° N–30° W | 0.56 ± 0.21 | GSFC (USA) | 0.98 ± 0.02 |
| Eurasia | 90° N–30° N 30° W–180° E | 0.54 ± 0.16 | Creteil (France) | 0.94 ± 0.03 |
| Central America | 30° N–0° 120° W–60° W | 0.43 ± 0.11 | Mexico City (Mexico) | 0.90 ± 0.02 |
| South America | 30° N–90° S 180° W–30° W | 0.35 ± 0.09 | Brazil | 0.91 ± 0.03 |
| Africa, Oceania | 30° N–90° S 30° W–180° E | 0.43 ± 0.17 | Mongu (Zambia) | 0.86 ± 0.015 |
| Indian Ocean | 30° E–120° E 30° N–10° S | 0.51 ± 0.15 | Maldives | 0.91 ± 0.03 |
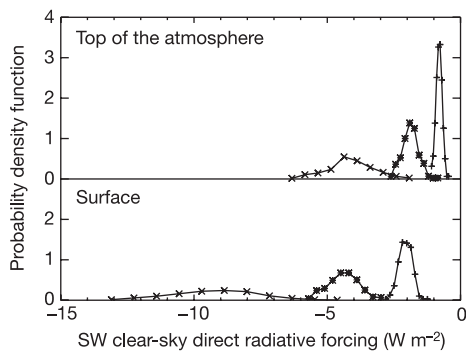
**Figure 3 | PDFs of the clear-sky shortwave aerosol DRF on an annual, global average.** Symbols are as used in Fig. 2a.

radiative effect of aerosols in cloudy sky, and is prima facie expected to compare well against the model estimates. However, there is a significant discrepancy between our clear-sky DRF ($-1.9\,\mathrm{W\,m^{-2}}$) and that from models ($-0.5$ to $-0.9\,\mathrm{W\,m^{-2}}$). Detailed comparisons with one such representative model revealed that the discrepancy stems from (in order of importance) too bright a surface albedo over both ocean and land in the model, too small an Ångström coefficient in the model, too small an optical thickness over land in the model, and to a smaller extent differences in global sampling, the radiative transfer code used to compute the radiative fluxes, the state of the mixture of the modelled aerosols and the vertical profiles of aerosol and water vapour. These results show that, although extreme negative values for the DRF are very unlikely, the DRF may be significantly stronger than current model estimates. Consequently, continued aerosol emission controls may lead to a stronger warming than current model predictions[10].

## METHODS

The PDFs are obtained from a set of 250 experiments. Each experiment derives an anthropogenic AOT and DRF. The algorithm uses daily data at the $1° \times 1°$ resolution from the MODIS products MOD08_D3. The MODIS AOT is corrected for the bias identified over both ocean and land surfaces[19]. Note that mineral dust and marine aerosol AOTs and DRFs are also estimated by the algorithm, but are left out of this study.

**Anthropogenic AOTs and DRFs.** Over ocean, the AMF retrieved by MODIS is reliable. Using the thresholds identified from Fig. 1, anthropogenic aerosols are immediately identified for AMFs larger than $0.83 \pm 0.05$. The total AOT is nevertheless corrected for a marine aerosol background optical thickness. For AMFs ranging from $0.35 \pm 0.05$ to $0.83 \pm 0.05$, grid-boxes with mixed mineral dust and biomass-burning aerosols are identified if the monthly averaged TOMS aerosol index is larger than $1.0 \pm 0.15$. The anthropogenic aerosol receives the accumulation-mode part of the total AOT after correcting for the marine background AOT. The assumption that the MODIS AMF is entirely of anthropogenic origin may be inaccurate for dust outbreaks over ocean areas where the AMF is typically 0.5. Over the Atlantic Ocean west of the Sahara, from May to September, such misidentifications are estimated to overestimate the global, annual-averaged anthropogenic AOT by at most 5%. The marine background AOT, $\tau_{\mathrm{marine}}$, is estimated from the SSM/I surface wind speed[9], $w$ (in $\mathrm{m\,s^{-1}}$), using $\tau_{\mathrm{marine}} = (0.006 \pm 0.001)w + (0.060 \pm 0.005)$. This formula is taken from the *in situ* measurements summarized in ref. 20. The standard deviations are chosen to make the gaussian distribution encompass the whole range of measured slopes and intercepts.

Over land, the AMF is unfortunately unreliable and is replaced by the anthropogenic fraction estimated from modelled anthropogenic and total AOT. The five global models we used participated in the AEROCOM project, and were run with the same prescribed emissions under pre-industrial and present-day conditions. The obtained regional values (Table 1) of the anthropogenic fraction are used to convert the total MODIS AOT to an anthropogenic AOT.

Aerosol size distributions and refractive indices are also needed to compute shortwave radiative fluxes at the top of the atmosphere and at the surface. Here, we use sun-photometer measurements from selected sites of the Aerosol Robotic

Network (AERONET)[12]. To account for the variability in aerosol properties, six regional boxes are defined and summarized in Table 1. Finally, we need to represent the surface albedo. Over oceans, the albedo depends on the solar zenith angle and the wavelength[21] and is calculated for a wind speed of $7\,\mathrm{m\,s^{-1}}$. Over land, it is computed from MODIS retrievals of the albedo for direct and diffuse radiation, with a different albedo in the visible and near-infrared spectra[22]. Surface albedo is adjusted for the aerosol effect on the distribution of downward radiation between the direct and diffuse fluxes. Radiative transfer calculations are performed using a discrete-ordinate solver[23], with 24 shortwave wavebands and 24 streams. Over ocean, the DRF is computed as the difference between radiative fluxes including the identified natural and anthropogenic aerosols and those including natural aerosols only. Over land, the DRF is computed as the difference between all aerosols and natural aerosols only, the former using the observed total optical depth, the latter using the total optical depth multiplied by one minus the anthropogenic fraction. The 24-hour-averaged DRF is computed by integrating the instantaneous radiative forcing over the solar zenith angles as a function of latitude and day of the year. Averages are weighted by the fraction of clear sky in a $1° \times 1°$ pixel (also termed pixel counts).

**Monte Carlo approach.** Most of the uncertainties in the uncertain algorithm parameters were previously given. We make one random choice constrained by our uncertainty assumptions for each global parameter (that is, threshold AMFs and aerosol regional SSA) and for each experiment. Similarly, we make multiple random choices subject to measurement errors for local parameters (that is, MODIS AOT, AMF and aerosol grid-box SSA) within each experiment. The MODIS total AOT at 0.55 mm, $\tau_{550}$, has a published uncertainty of $\pm 0.03 \pm 0.05\tau_{550}$ over ocean, and $\pm 0.05 \pm 0.15\tau_{550}$ over land[19]. The MODIS AMF has a large uncertainty of $\pm 0.25$.

1.  Ramaswamy, V. *et al.* (ed.) *Climate Change 2001: The Scientific Basis. Contribution of WGI to the Third Assessment Report of the IPCC* (Cambridge Univ., Cambridge, 2001).
2.  Reddy, M. S. *et al.* Estimates of global multi-component aerosol optical depth and direct radiative perturbation in the LMDZT General Circulation Model. *J. Geophys. Res.* 110, doi:10.1029/2004JD004757 (2005).
3.  Roberts, D. L. & Jones, A. Climate sensitivity to black carbon aerosol from fossil fuel combustion. *J. Geophys. Res.* 109, doi:10.1029/2004JD004676 (2004).
4.  Bellouin, N., Boucher, O., Tanré, D. & Dubovik, O. Aerosol absorption over the clear-sky oceans deduced from POLDER-1 and AERONET observations. *Geophys. Res. Lett.* 30, doi:10.1029/2003GL017121 (2003).
5.  Christopher, S. A. & Zhang, J. Shortwave aerosol radiative forcing from MODIS and CERES observations over the oceans. *Geophys. Res. Lett.* 29, doi:10.1029/2002GL014803 (2002).
6.  Kaufman, Y. J. *et al.* Operational remote sensing of tropospheric aerosol over land from EOS moderate resolution imaging spectroradiometer. *J. Geophys. Res.* 102, 17051–17068 (1997).
7.  Tanré, D., Kaufman, Y. J., Herman, M. & Mattoo, S. Remote sensing of aerosol properties over oceans using the MODIS/EOS spectral radiances. *J. Geophys. Res.* 102, 16971–16988 (1997).
8.  Herman, J. R. *et al.* Global distribution of UV-absorbing aerosols from Nimbus 7/TOMS data. *J. Geophys. Res.* 102, 16911–16922 (1997).
9.  Wentz, F. A well calibrated ocean algorithm for SSM/I. *J. Geophys. Res.* 102, 8703–8718 (1997).
10. Andreae, M. O., Jones, C. D. & Cox, P. M. Strong present-day aerosol cooling implies a hot future. *Nature* 435, 1187–1190 (2005).
11. Osborne, S. R. & Haywood, J. M. Aircraft observations of the physical and optical properties of major aerosol types. *Atmos. Res.* 73, 173–201 (2005).
12. Dubovik, O. *et al.* Variability of absorption and optical properties of key aerosol types observed in worldwide locations. *J. Atmos. Sci.* 59, 590–608 (2002).
13. Takemura, T., Nozawa, T., Emori, S., Nakajima, T. Y. & Nakajima, T. Simulation of climate response to aerosol direct and indirect effects with aerosol transport-radiation model. *J. Geophys. Res.* 110, doi:10.1029/2004JD005029 (2005).
14. Collins, W. D. *et al.* Simulation of aerosol distributions and radiative forcing for INDOEX: Regional climate impacts. *J. Geophys. Res.* 107, doi:10.1029/2000JD000032 (2002).
15. Stier, P. *et al.* The aerosol-climate model ECHAM5-HAM. *Atmos. Chem. Phys.* 5, 1125–1156 (2005).
16. Kirkevåg, A. & Iversen, T. Global direct radiative forcing by process-parameterized aerosol optical properties. *J. Geophys. Res.* 107, doi:10.1029/2001JD000886 (2002).
17. Platnick, S. *et al.* The MODIS cloud products: algorithms and examples from Terra. *IEEE Trans. Geosci. Remote Sens.* 41, 459–473 (2003).
18. Keil, A. & Haywood, J. M. Solar radiative forcing by biomass aerosol particles over marine clouds during SAFARI-2000. *J. Geophys. Res.* 108, doi:10.1029/2002JD002315 (2003).

19. Remer, L. A. *et al.* The MODIS aerosol algorithm, products, and validation. *J. Atmos. Sci.* **62**, 947–973 (2005).
20. Smirnov, A., Holben, B. N., Eck, T. F., Dubovik, O. & Slutsker, I. Effect of wind speed on columnar aerosol optical properties at Midway Island. *J. Geophys. Res.* **108**, doi:10.1029/2003JD003879 (2003).
21. Cox, C. & Munk, W. Statistics of the sea surface derived from sun glitter. *J. Mar. Res.* **13**, 198–227 (1954).
22. Schaaf, C. B. *et al.* First operational BRDF, albedo nadir reflectance products from MODIS. *Remote Sens. Environ.* **83**, 135–148 (2002).
23. Key, J. R. & Schweiger, A. J. Tools for atmospheric radiative transfer: STREAMER and FLUXNET. *Comput. Geosci.* **24**, 443–451 (1998).